図4 *Rev1*ホモマウスにおけるTCR 突然変異体頻度の検出

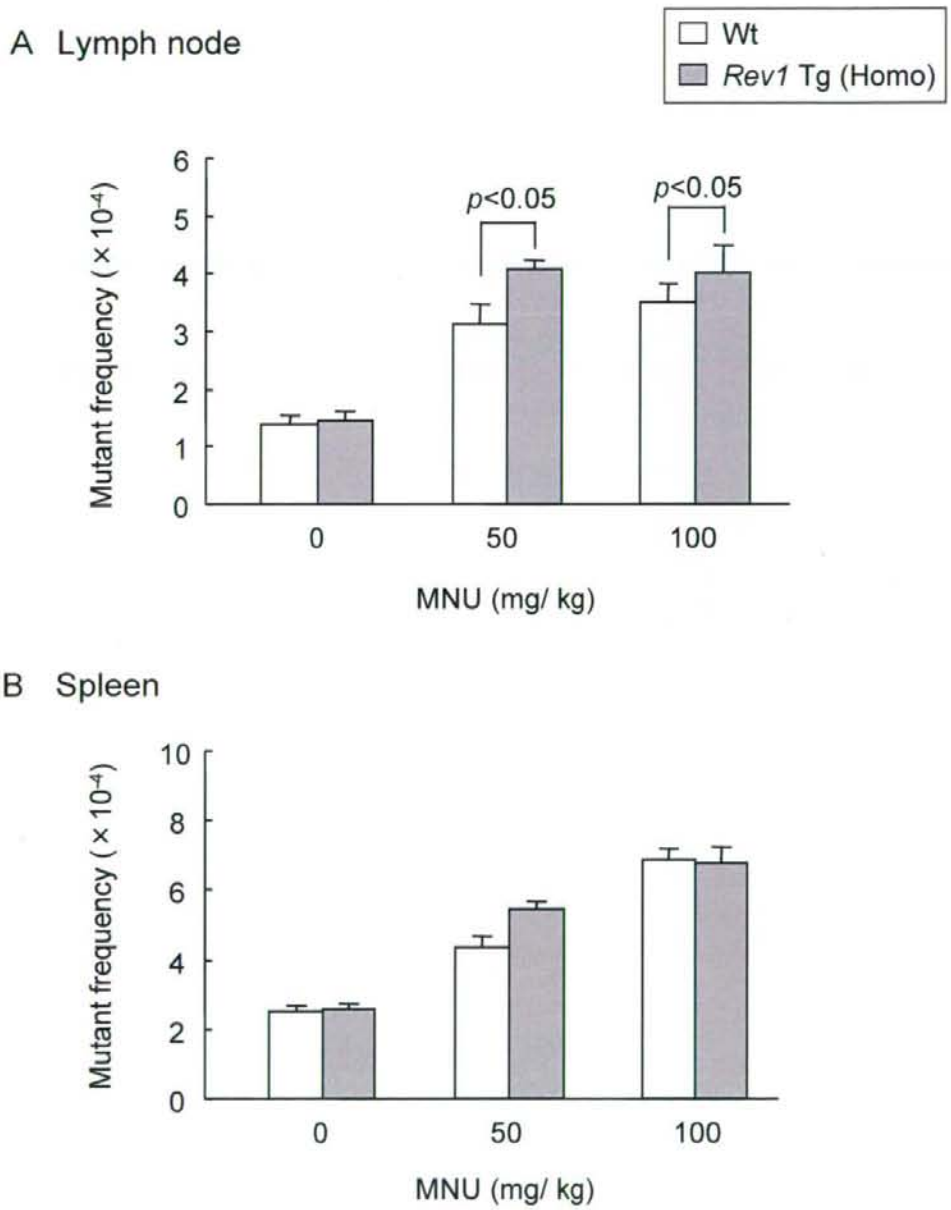

図5 *Rev1*ホモマウスに誘発された小腸腺癌

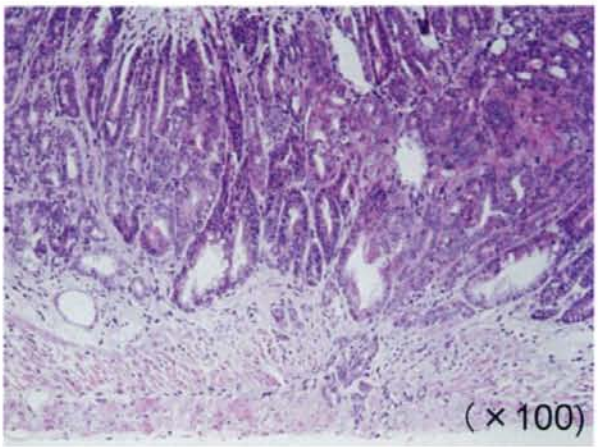

図6 *Rev1*ホモマウスの小腸での*Rev1* mRNAの発現

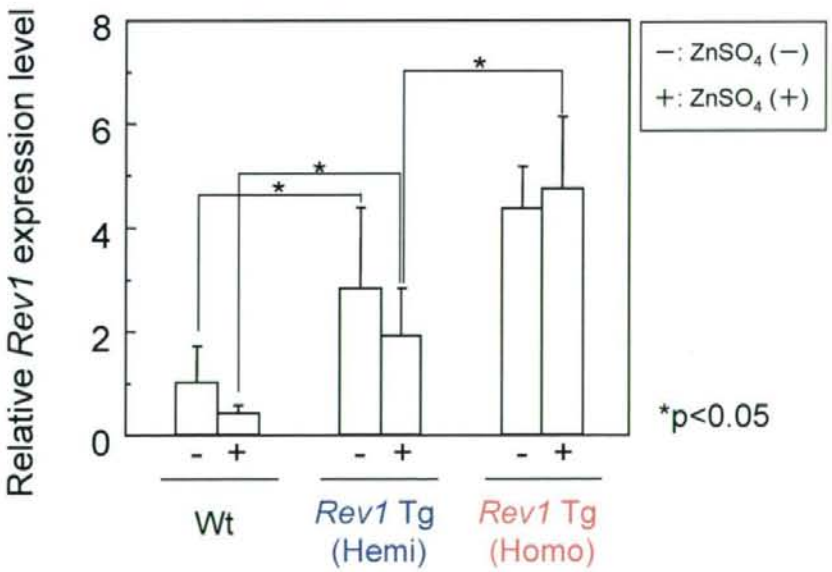

図7 *Rev1*ホモマウスの短期発がん試験での小腸腫瘍の誘発

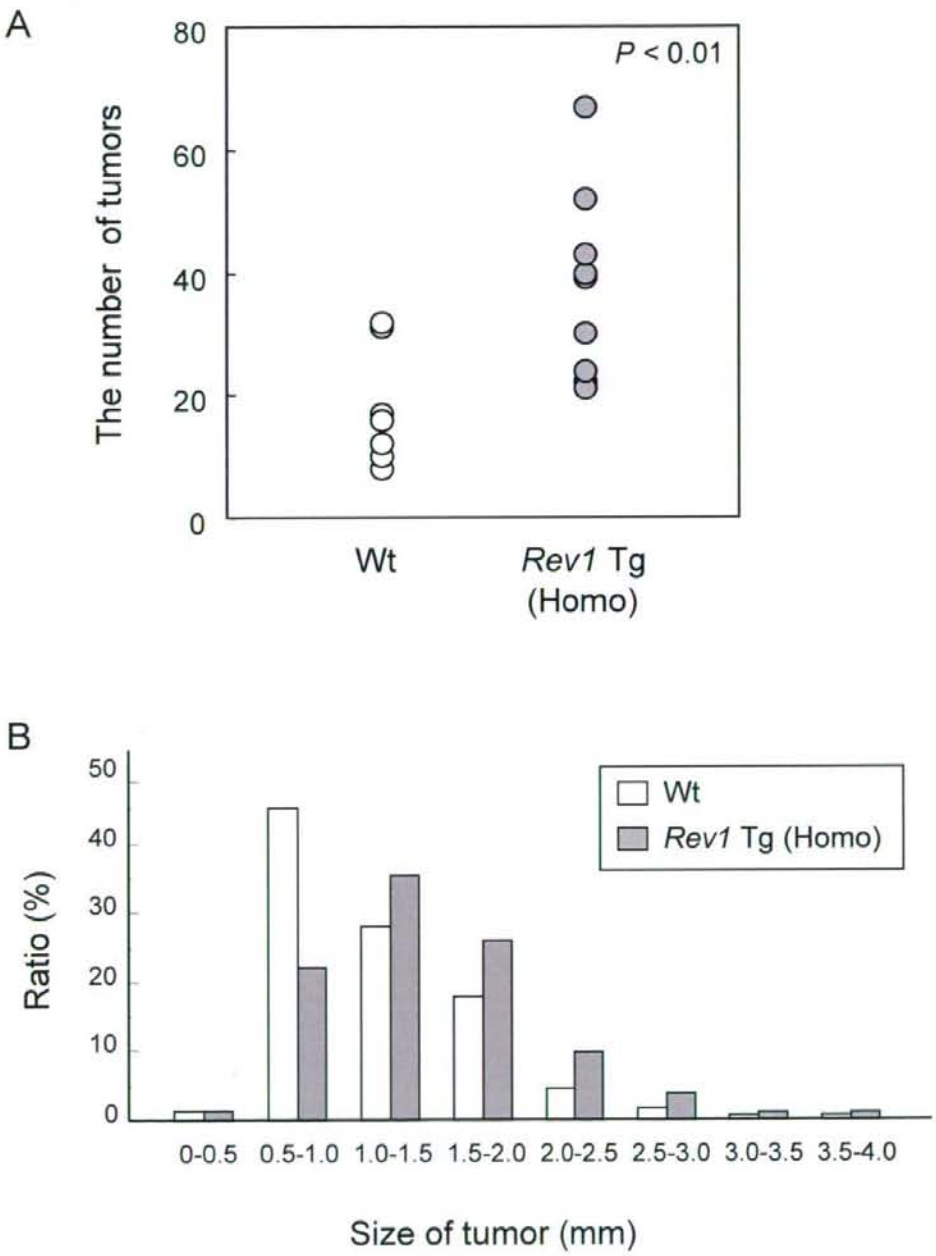

図8 *Rev1* マウスの小腸に誘発されたmicro-adenoma（Ⅰ）

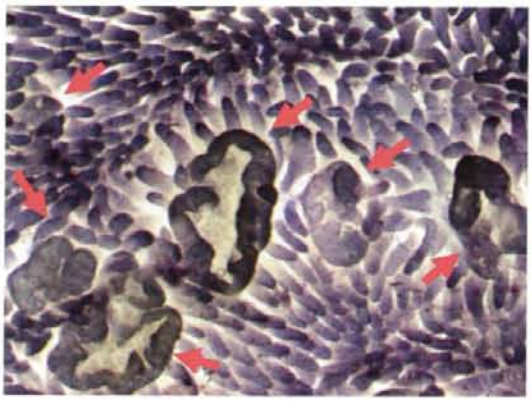

アルカリフォス
ファターゼ染色

図9 *Rev1* マウスの小腸に誘発されたmicro-adenoma（Ⅱ）

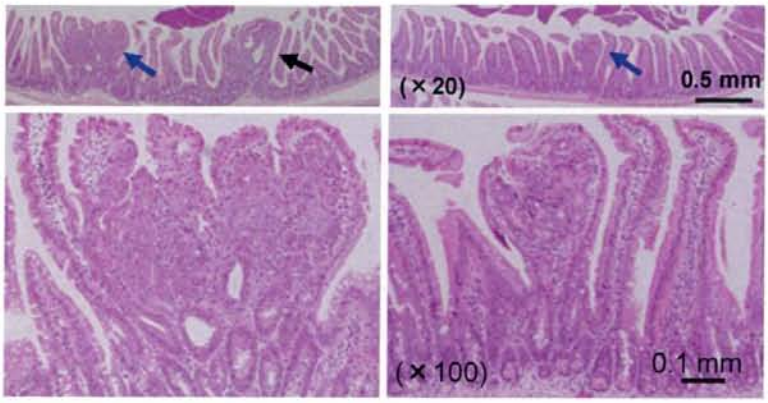

HE染色

図10 *Rev1* ホモマウスの1ヶ月間発がん試験

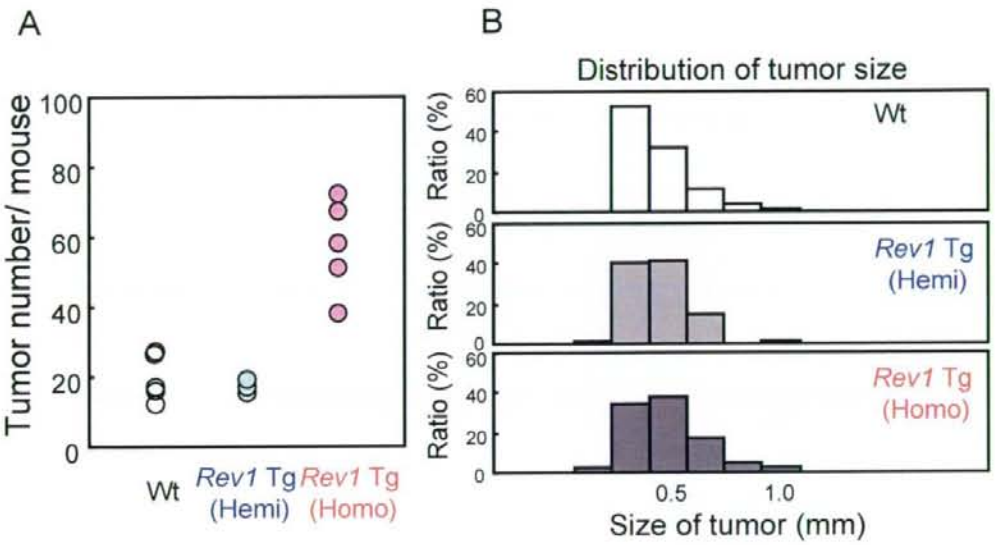

図11 *Rev1* ホモマウスの2ヶ月間発がん試験

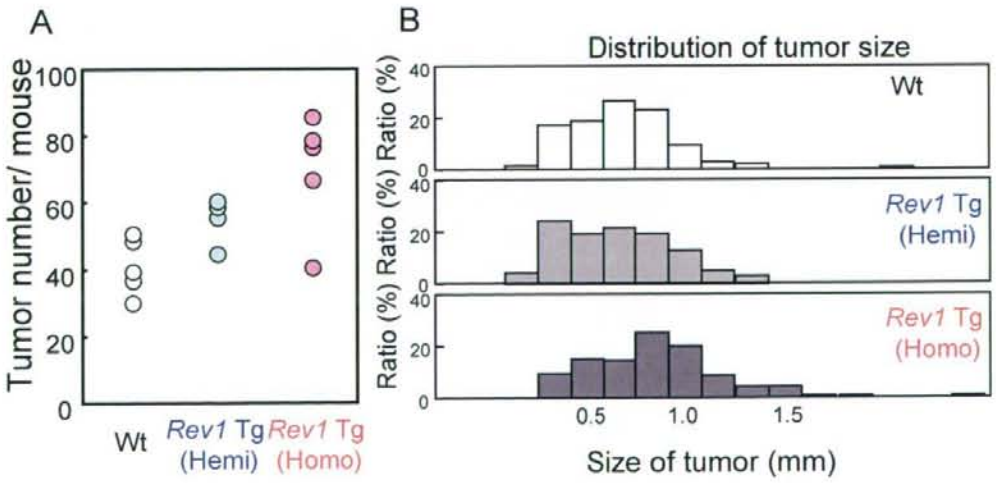

図12　MNU投与により誘発された胸腺リンパ腫のゲノムDNAを用いた
aCGH解析による*c-Myc*を含む15番染色体の増幅

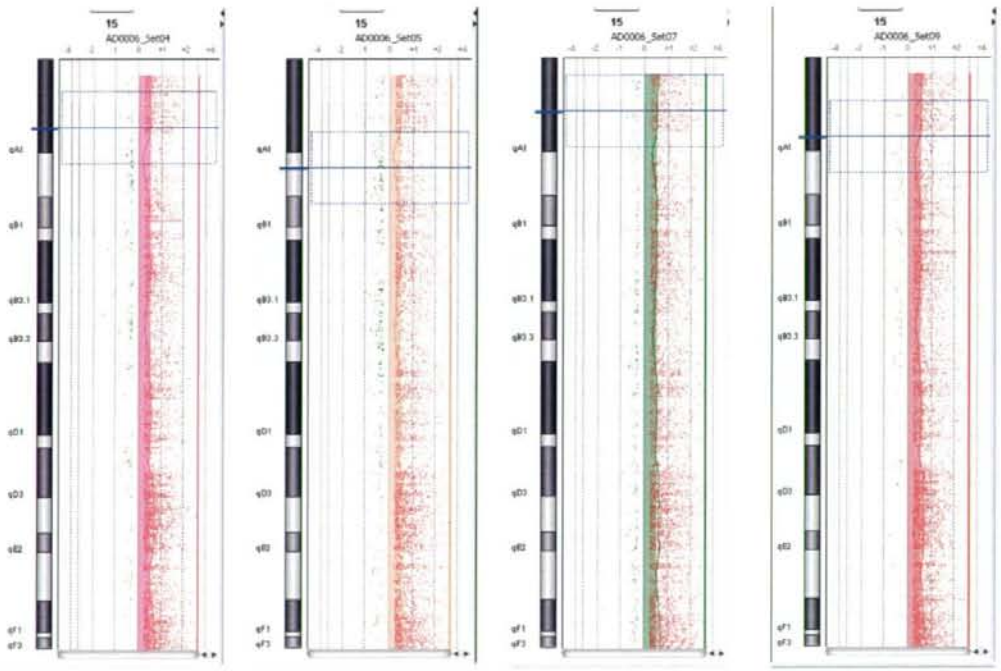

図13　MNU投与により誘発された胸腺リンパ腫のゲノムDNAを用いた
aCGH解析による*TCRβ*を含む6番染色体qB1の欠失

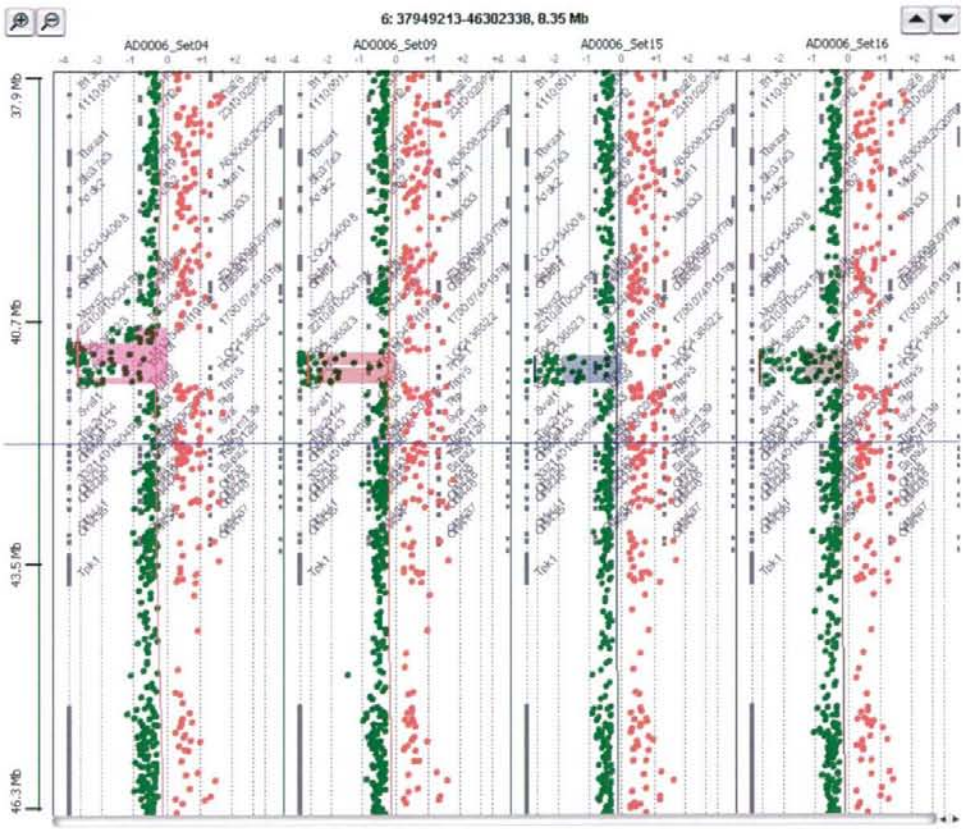

図14　MNU投与により誘発された胸腺リンパ腫のゲノムDNAを用いた
aCGH解析による14番染色体qC1の欠失

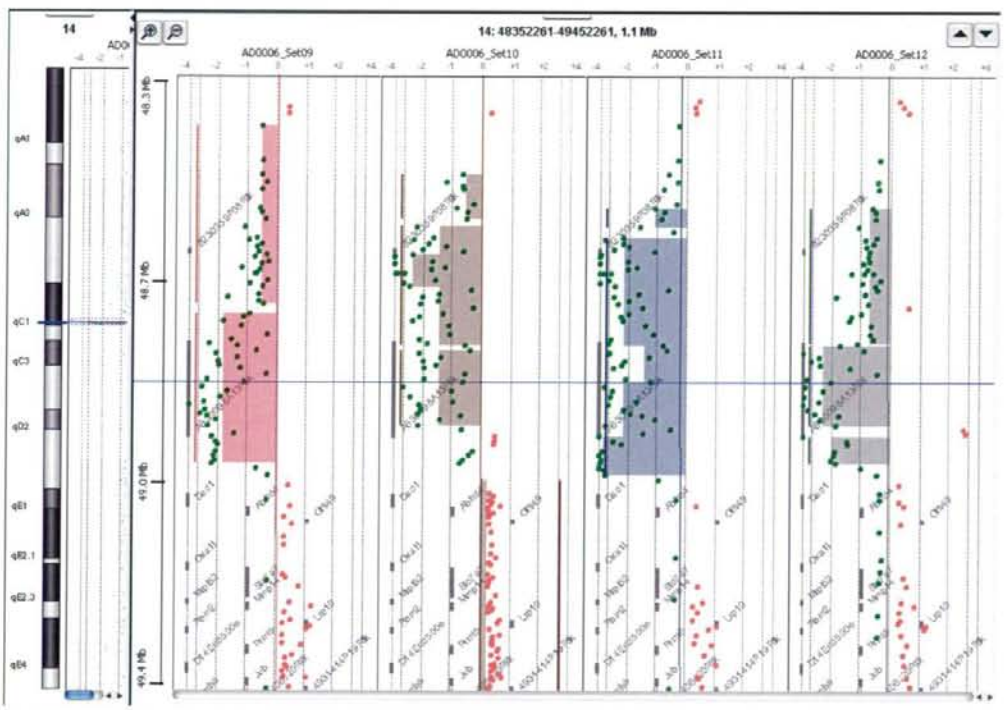

図15-1 雄*Rev1*ホモマウスの体重の推移(ばい煎ダイズ抽出物の1年間反復投与毒性試験)

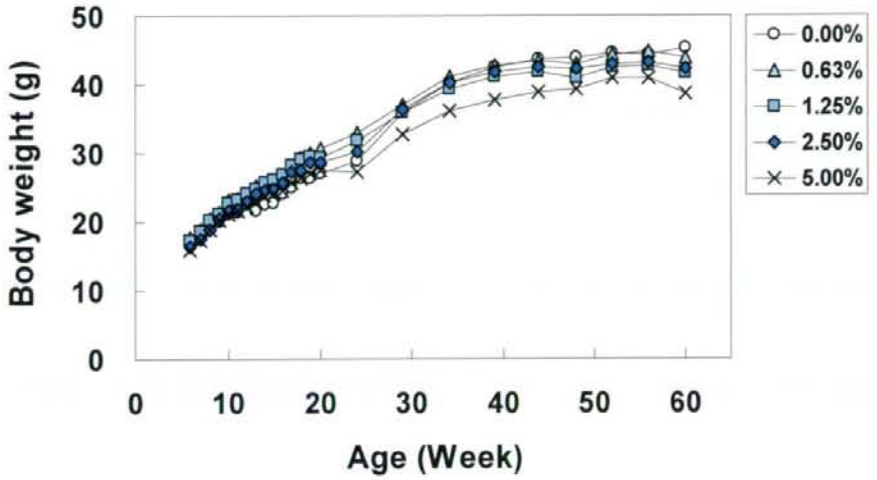

図15-2 雌*Rev1*ホモマウスの体重の推移(ばい煎ダイズ抽出物の1年間反復投与毒性試験)

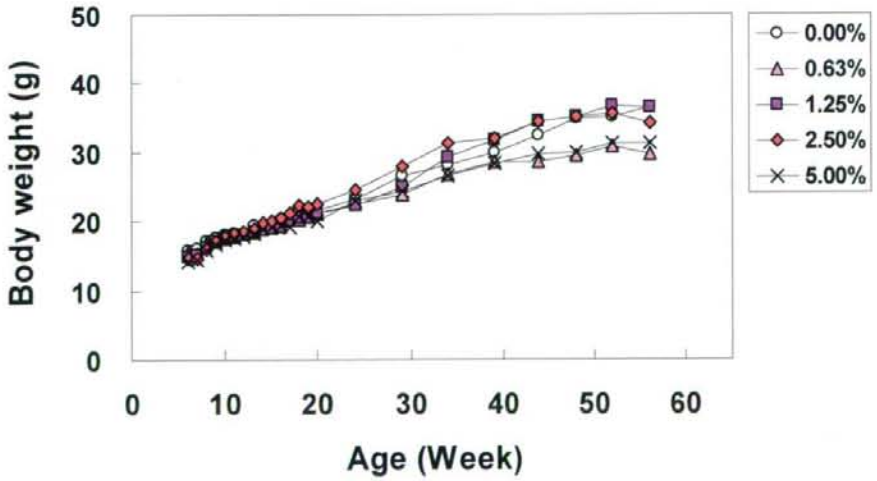

図16-1 雄*Rev1*ホモマウスの平均摂餌量(ばい煎ダイズ抽出物の1年間反復投与毒性試験)

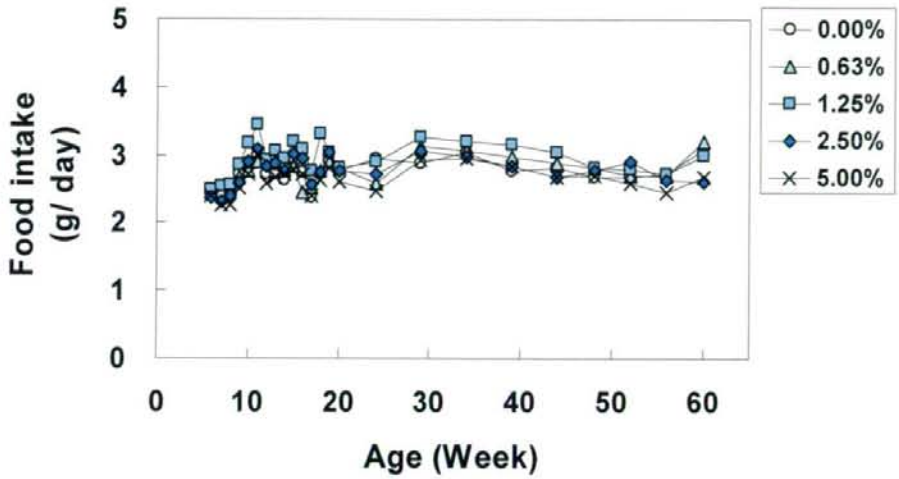

図16-2 雌*Rev1*ホモマウスの平均摂餌量(ばい煎ダイズ抽出物の1年間反復投与毒性試験)

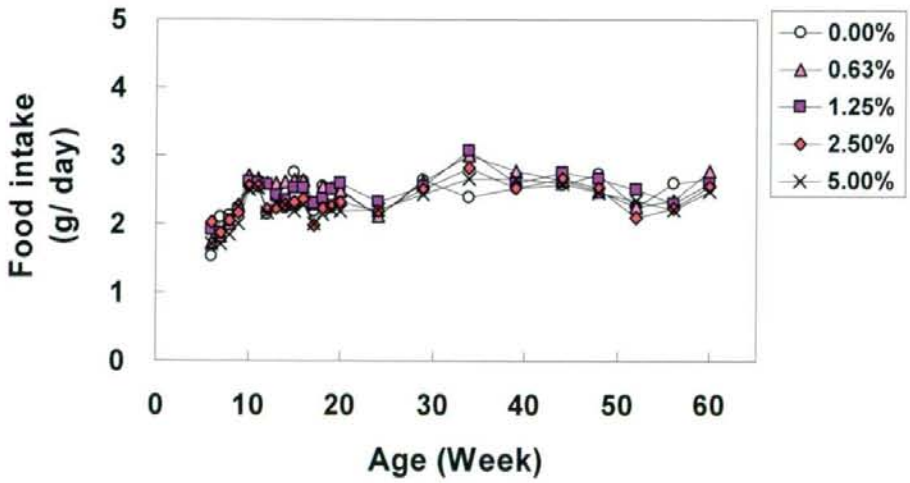

図17-1 雄*Rev1*ホモマウスの平均摂水量(ばい煎ダイズ抽出物の1年間反復投与毒性試験)

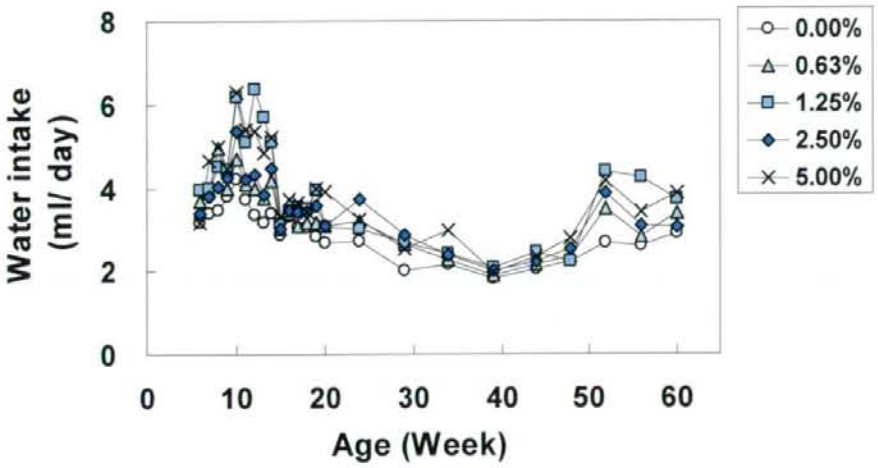

図17-2 雌*Rev1*ホモマウスの平均摂水量(ばい煎ダイズ抽出物の1年間反復投与毒性試験)

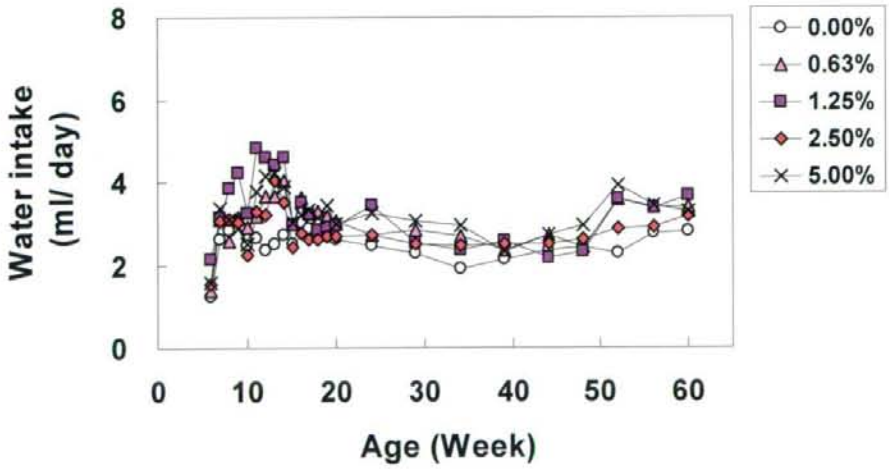

別紙4

研究成果の刊行に関する一覧表

雑誌

発表者氏名	論文タイトル名	発表誌名	巻号	ページ	出版年
Ikura, T., Tashiro, S., Kakino, A., Shima, H., Jacob, N., Amunugama, R., Yoder, K., Izumi, S., Kuraoka, I., Tanaka, K., Kimura, H., Ikura, M., Nishikubo, S., Ito, T., Muto, A., Miyagawa, K., Takeda, S., Fishel, R., Igarashi, K., Kamiya, K	DNA damage-dependent acetylation and ubiquitination of H2AX enhances chromatin dynamics	Mol Cell Biol	27(20)	7028-7040	2007
Masuda, Y., Suzuki, M., Piao, J.L., Gu, Y.Q., Tsurimoto, T., Kamiya, K	Dynamics of human replication factors in the elongation phase of DNA replication	Nucl. Acids Res.	35(20)	6904-6916	2007
Tomida, J., Masuda, Y., Hiroaki, H., Ishikawa, T., Song, I., Tsurimoto, T., Tateishi, S., Shiomi, T., Kamei, Y., Kim, J., Kamiya, K., Vaziri, C., Ohmori, H., Todo, T	DNA damage induced ubiquitylation of RFC2 subunit of RFC complex	J. Biol. Chem.	283(14)	9071-9079	2008
朴金蓮, 増田雄司, 神谷研二	ヒトREV1による損傷乗り越えDNA合成の生化学的解析	広島医学	61(4)	338-339	2008
Yoshihiko Uehara, Hironobu Ikehata, Jun-ichro Komura, Ari Ito, Masaki Ogata, Tsunetoshi Itoh, Ryoichi Hirayama, Yoshiya Furusawa, Koichi Ando, Tatjana Panuesku, Cayle E. Woloschak, Kenshi Komatsu, Shinya Matsuura, Tsuyoshi Ikura, Kenji Kamiya and Tetsuya Ono	Absence of Ku70 Gene Obliterates X-Ray-Induced lacZ Mutagenesis of Small Deletions in Mouse Tissues	Radiation Research	170(2)	216-223	2008
増田雄司, 神谷研二	誘発突然変異と損傷乗り越えDNA合成ーREV1の構造と生化学的機能ー	生化学	80(9)	843-846	2008
Gu, Y.Q., Masuda, Y., Kamiya, K	Biochemical analysis of human PIF1 helicase and functions of its N-terminal domain	Nucleic Acids Research	36(19)	6295-6308	2008

MOLECULAR AND CELLULAR BIOLOGY, Oct. 2007, p. 7028–7040
0270-7306/07/$08.00+0 doi:10.1128/MCB.00579-07

Vol. 27, No. 20

DNA Damage-Dependent Acetylation and Ubiquitination of H2AX Enhances Chromatin Dynamics▽†

Tsuyoshi Ikura,[1]*‡ Satoshi Tashiro,[2]‡ Akemi Kakino,[4] Hiroki Shima,[2] Naduparambil Jacob,[5] Ravindra Amunugama,[5] Kristine Yoder,[5] Shunsuke Izumi,[6] Isao Kuraoka,[7] Kiyoji Tanaka,[7] Hiroshi Kimura,[8] Masae Ikura,[1] Shuichi Nishikubo,[4] Takashi Ito,[9] Akihiko Muto,[1] Kiyoshi Miyagawa,[3] Shunichi Takeda,[10] Richard Fishel,[5] Kazuhiko Igarashi,[1] and Kenji Kamiya[4]*

Department of Biochemistry, Tohoku University Graduate School of Medicine, Seiryoumachi 2-1, Aobaku Sendai 980-8575, Japan[1]; Department of Cellular Biology,[2] Department of Human Genetics,[3] and Department of Experimental Oncology,[4] RIRBM, Hiroshima University, Hiroshima 734-8553, Japan; Molecular Virology, Immunology and Medical Genetics, Human Cancer Genetics, The Ohio State University School of Medicine and Public Health, Columbus, Ohio 43210[5]; Graduate School of Science and The Center for Quantum Life Science, Hiroshima University, 1-3-1 Kagamiyama, Higashihiroshima 739-8526, Japan[6]; Graduate School of Frontier Biosciences, Osaka University, 1-3 Yamada-oka, Suita, Osaka 565-0871, Japan[7]; Nuclear Function and Dynamics Unit, HMRO, School of Medicine, Kyoto University, Yoshida Konoe-cho, Sakyo-ku, Kyoto 606-8501, Japan[8]; Department of Biochemistry, Nagasaki University School of Medicine, Nagasaki 852-8523, Japan[9]; and CREST Laboratory, Department of Radiation Genetics, Kyoto University Graduate School of Medicine, Kyoto 606-8501, Japan[10]

Received 2 April 2007/Returned for modification 17 May 2007/Accepted 2 August 2007

Chromatin reorganization plays an important role in DNA repair, apoptosis, and cell cycle checkpoints. Among proteins involved in chromatin reorganization, TIP60 histone acetyltransferase has been shown to play a role in DNA repair and apoptosis. However, how TIP60 regulates chromatin reorganization in the response of human cells to DNA damage is largely unknown. Here, we show that ionizing irradiation induces TIP60 acetylation of histone H2AX, a variant form of H2A known to be phosphorylated following DNA damage. Furthermore, TIP60 regulates the ubiquitination of H2AX via the ubiquitin-conjugating enzyme UBC13, which is induced by DNA damage. This ubiquitination of H2AX requires its prior acetylation. We also demonstrate that acetylation-dependent ubiquitination by the TIP60-UBC13 complex leads to the release of H2AX from damaged chromatin. We conclude that the sequential acetylation and ubiquitination of H2AX by TIP60-UBC13 promote enhanced histone dynamics, which in turn stimulate a DNA damage response.

Chromatin reorganization by histone modification and mobilization plays a crucial role in DNA metabolism, including replication, transcription, and repair. It appears that histone modification and mobilization can reorganize chromatin to allow DNA repair machinery to access damaged chromosomal DNA (11, 29, 52, 56, 57).

H2AX is a histone variant that differs from H2A at various amino acid residues along the entire protein and in its C-terminal extensions. H2AX is phosphorylated after the induction of DNA double-strand breaks (DSBs), and the phosphorylated H2AX (γ-H2AX) participates in focus formation at sites of DNA damage. After induction of DSBs, the MRN complex (*M*RE11, *R*AD50, and *N*BS1) binds to broken DNA ends and recruits active ATM, ATR, and/or DNA protein kinase, resulting in the initial phosphorylation of H2AX (32, 38, 40). MDC1 then associates with γ-H2AX and recruits additional activated ATM to the sites of DSBs (23, 46). This positive feedback loop leads to the expansion of the γ-H2AX region surrounding DSBs and provides docking sites for many DNA damage and repair proteins, including the MRN complex, 53BP1, and BRCA1 (5, 6, 46). γ-H2AX plays a role in the accumulation but not in the initial recruitment of repair factors such as the MRN complex, 53BP1, and BRCA1 (10, 63). Therefore, modifications of H2AX other than phosphorylation could play a role in the initial step of the DNA damage response.

Until recently, the biological significance of ubiquitination in the DNA damage response has been unclear. H2B ubiquitination regulates the damage checkpoint response (15). H2A is ubiquitinated during the response to UV-induced DNA damage (8). UV-induced DNA damage also causes the ubiquitination of histones H3 and H4, resulting in their release from chromatin (60). Interestingly, ubiquitin-conjugated proteins appear to be accumulated at sites of DSBs, forming nuclear foci like γ-H2AX (34). These findings raise the possibility that histone ubiquitination is also involved in the reorganization of chromatin in response to DSBs. To date, how the ubiquitination of histones is organized in the DNA damage response remains unknown.

* Corresponding author. Mailing address for Tsuyoshi Ikura: Department of Biochemistry, Tohoku University Graduate School of Medicine, Seiryoumachi 2-1, Aobaku Sendai 980-8575, Japan. Phone: 81-022-717-7597. Fax: 81-022-717-7598. E-mail: ikurat@mail.tains.tohoku.ac.jp. Mailing address for Kenji Kamiya: Department of Experimental Oncology, RIRBM, Hiroshima University, Hiroshima 734-8553, Japan. Phone: 81-082-257-5842. Fax: 81-082-257-5844. E-mail: kkamiya@hiroshima-u.ac.jp.

† Supplemental material for this article may be found at http://mcb.asm.org/.

‡ These authors contributed equally to this work.

▽ Published ahead of print on 20 August 2007.

We and other groups have shown that the histone acetyltransferase (HAT) TIP60/Esa1 participates in the DNA damage response as a protein complex (9, 13, 16, 30, 54, 55). For example, TIP60 induces histone H4 acetylation and the accumulation of repair molecules, including RAD51, at sites of DSBs with TRRAP in human cells (30). In *Saccharomyces cerevisiae*, the NuA4 complex, including Esa1, a yeast homologue of human TIP60, binds histone H4 through Arp4 to mediate the DSB-induced acetylation of H4 (9). However, it is not yet known how histone acetylation by the TIP60 complex regulates chromatin organization immediately after the induction of DSBs in the human DNA repair response.

In addition to histone modifications, histone eviction/release and histone variant exchange can facilitate DNA repair by recruiting signaling and repair factors (12, 25, 57). The exchange of core histones for a specific variant within nucleosomes can also alter chromatin structure in a temporally controlled manner (1, 3, 19, 22, 26, 28, 42, 49, 62). For example, *Drosophila melanogaster* DmTIP60 has been shown to acetylate phospho-H2A.v in vitro, resulting in its removal from chromatin due to exchange with an unmodified H2A.v (22). In budding yeast, H2A (or phospho-H2A) is replaced with the H2A variant Htz1 by the histone exchange complex SWR1 (28). The INO80 complex provokes chromatin reorganization following DNA damage; this reorganization includes the release of histones H2B and H3 at sites around DSBs, leading to the recruitment of RAD51 (29, 53). Furthermore, the histone variant H3.1 appears to be deposited at sites of UV damage by the chromatin assembly factor CAF-1 (36). Although these studies indicate that histone eviction and variant exchange are important mechanisms for altering chromatin structure during the DNA damage response (35, 57), it is not clear how histone modifications engage in these chromatin reorganizations immediately following the induction of DSBs during DNA repair in human cells.

Here, we show that the TIP60 HAT complex interacts with H2AX immediately after exposure to ionizing irradiation (IR). Furthermore, DSBs facilitate the association of TIP60 with the ubiquitin-conjugating enzyme UBC13 (2). The TIP60-UBC13 complex regulates the acetylation and ubiquitination of H2AX following the formation of DSBs. The DSB-induced acetylation of H2AX lysine 5 (K5) is required for this ubiquitination and occurs independently of the phosphorylation of H2AX. We also show that damage-induced acetylation and ubiquitination provoke the release of H2AX from chromatin immediately after the induction of DSBs. Because TIP60-UBC13 is required for the DSB-induced ubiquitination and release of H2AX, these findings provide the first evidence that human TIP60 promotes the acetylation-dependent ubiquitination of H2AX by UBC13, causing H2AX release from chromatin, which facilitates chromatin reorganization following DNA damage.

MATERIALS AND METHODS

Cell culture. HeLa cells (16) (kind gift from Y. Nakatani, Dana-Faber Cancer Institute) and GM02063 (51), a simian virus 40-transformed human fibroblast cell line, were cultured in Dulbecco's modified Eagle's medium supplemented with 10% fetal calf serum.

Reagents and antibodies. Anti-FLAG and antihemagglutinin (anti-HA) antibody-conjugated agaroses (Sigma) were used for the purification of FLAG-HA-tagged proteins. Immunoblotting analyses were performed with anti-TIP60 (Upstate), anti-acetylated H2A(K5) (Cell Signaling), anti-glyceraldehyde-3-phosphate dehydrogenase (anti-GAPDH) (Santa Cruz Biotechnology), anti-FLAG (Sigma), anti-H2AX (Sigma), antiubiquitin (FK2; Nippon Bio-Test Lab), anti-UBC13 (Zymed), and anti-HA (Roche) antibodies.

Affinity purification of H2AX and TIP60 complexes. HeLa cells expressing FLAG-HA epitope-tagged H2AX (eH2AX; wild type or site-specific mutants) or TIP60 (eTIP60) were grown to 1.0×10^6 cells/ml as suspension cultures. For the induction of DNA damage, cells were γ-irradiated (12 Gy) after centrifugation. The nuclear extract and chromatin fraction were prepared from the cells, and the H2AX and TIP60 complexes were purified from the nuclear extracts as previously described (16, 31). To affinity purify eH2AX (wild type and mutants) from the chromatin fraction, the nuclear pellet was resuspended in a buffer of 20 mM Tris-HCl (pH 8.0), 500 mM KCl, 5 mM $MgCl_2$, 0.2 mM EDTA, 10% glycerol, 0.1% Tween 20, 10 mM 2-mercaptoethanol, and 0.25 mM phenylmethylsulfonyl fluoride and then lysed by sonication. After the removal of insoluble material by centrifugation, eH2AX and eTIP60 were affinity purified (16, 31).

Microirradiation, FRAP, and iFRAP. GM02063 cells expressing green fluorescent protein (GFP)-tagged H2AX (GFP-H2AX; wild type or site-specific mutants), H2A (GFP-H2A), H2B (GFP-H2B), H3 (GFP-H3), or H4 (GFP-H4) were maintained on the microscope stage in an FCS live-cell chamber system (Bioptechs) at 37°C. Imaging, microirradiation, and fluorescence recovery after photobleaching (FRAP) experiments were performed using an LSM510 confocal microscope (Carl Zeiss). For microirradiation, sensitization of cells was performed by incubating the cells for 20 h in medium containing 2.5 μM deoxyribosylthymine and 0.3 μM bromodeoxyuridine (Sigma) and then staining with 2 μg/ml Hoechst 33258 (Sigma) for 10 min before UVA microirradiation as described previously (58). The 364-nm line of the UVA laser was used for microirradiation (three pulses at 180 μW). The maximum power of the 488-nm Ar laser line was used for photobleaching in FRAP analysis. For imaging, the laser was attenuated to 0.1%. For inverse FRAP (iFRAP) experiments (14, 37), photobleaching was performed under the same conditions as for FRAP analysis. All fluorescence regions except for small regions in irradiated and unirradiated areas were bleached, and the remaining GFP fluorescence was chased using the LSM510 confocal microscopy. For FRAP and iFRAP analysis, a prebleached image was acquired just after the induction of DSBs by UVA laser microirradiation, after which the bleaching pulse was delivered. To quantify fluorescence recovery, single optical sections were collected at 3- or 5-s intervals for the indicated periods of time. Image J was used for the quantification of fluorescent intensity in FRAP analysis. Background fluorescence intensity (BG) was measured in a random field outside of the cells. The average fluorescence intensity in the bleached region at each time point (I_t) was measured in a region corresponding to at least 30% of the bleached region. For each time point, the relative intensity was calculated as follows: $I_{rel,t} = (I_t - BG)/(I_0 - BG)$, where I_0 is the average intensity of the region of interest before bleaching. The percent recovery after 260 s in FRAP analysis ($P_{recovery,260\ s}$) was calculated as follows: $P_{recovery,260\ s} = 100 \times (I_{rel,260\ s} - I_{rel,6\ s})/(1 - I_{rel,6\ s})$, where $I_{rel,6\ s}$ is the relative intensity of the bleached area in the first image taken after bleaching (6 s after bleaching), and $I_{rel,260\ s}$ is the relative intensity of the bleached area in the image taken 260 s after bleaching. Statistical comparisons were made using Student's t test. Image J was also used to generate profile plots of fluorescence intensity in the iFRAP analysis.

Immunofluorescence analysis. Cells were fixed with 4% paraformaldehyde in 1× phosphate-buffered saline (PBS). Next, nuclei were permeabilized with 0.1% sodium dodecyl sulfate (SDS)–0.5% Triton X-100 in 1× PBS for 5 min. An in situ cell death detection kit (Roche) was used for the terminal deoxynucleotidyltransferase-mediated dUTP-biotin nick end labeling (TUNEL) technique as recommended by the manufacturer. For the detection of RAD51, fixed cells were incubated for 30 min at 37°C with anti-RAD51 antibody (1:2,000; kindly provided by A. Shinohara, Osaka University) in 1% bovine serum albumin-1× PBS. Fluorescein isothiocyanate-conjugated goat anti-rabbit (1:1,000; Biosource) was used as the secondary antibody. Nuclei were stained with Hoechst 33342. Samples were examined with an Axioplan2 microscope and using an AxioCam MRm controlled by Axiovision (Zeiss).

MS-MS analysis. Protein sequences were determined using an ultraflex time-of-flight mass spectrometer (Bruker Daltonics) equipped with a nitrogen laser operating at 337 nm. The samples were also examined by tandem mass spectroscopy (MS-MS) methods with an AXIMA-QIT (Shimazu-Kratos) ion trap matrix-assisted laser desorption mass spectroscopy (MS). The following sequences were extracted: for TIP60, N'-EVPASAQASGK-C', N'-LFYVHYIDFNK-C', N'-LLIEFSYELSKVEGK-C', and N'-EDVISTLQYLNLINYYK-C'; for Ub-H2AX, N'-AGLQFPVGR-C', N'-ESTLHLVLR-C', N'-K(LRGG)TSATVGPK-C', and

N'-HLQLAIRNDEELN-C'; and for H2AX, N'-HLQLAIR-C', N'-AGLQFPV GR-C', and N'-LLGGVTIAQGGVLPNIQAVLLPK-C'.

siRNA. The short interfering RNA (siRNA) expression vector pSUPER. retro.puro (OligoEngine) was used to knock down TIP60 (target sequence, 5'-GGACATCAGTGGCCGGAAGC-3' [siTIP60.1] or 5'-ACGGAAGGTGGA GGTGGT-3' [siTIP60.2]), H2AX (5'-CTGGAATTCTGCAGCTAAC-3'), or UBC13 (5'-AAGCATGAGCAGAGGCTAGAA-3' [siUBC13.1] or 5'-AAGCA GCTAACCAGGTCTTTA-3' [siUBC13.2]). Retroviral production was used to generate GM02063 cells or HeLa cells stably expressing TIP60-, H2AX-, and UBC13-specific or control siRNAs based on puromycin resistance. To measure the levels of proteins, cells were lysed in protein sample buffer and analyzed by immunoblotting.

RESULTS

TIP60 HAT regulates DNA damage-induced acetylation of H2AX. To identify proteins that associate with H2AX immediately after the induction of DNA damage, stably expressed FLAG-HA eH2AX was purified from nuclear extracts of HeLa cells following treatment with IR. Purification of eH2AX was performed by sequential steps of affinity chromatography on anti-FLAG antibody-conjugated agarose followed by anti-HA antibody-conjugated agarose (16, 31), and the associated proteins were analyzed by SDS-polyacrylamide gel electrophoresis. SDS-polyacrylamide gel electrophoresis analysis of the purified H2AX complexes indicated that several proteins are associated with H2AX in a DNA damage-dependent manner (see Fig. S1A in the supplemental material). We employed MS analysis to identify the binding partner of H2AX. MS analysis indicated that TIP60 HAT was included in the purified H2AX complex following the induction of DNA damage by IR. This was confirmed by immunoblotting with an anti-TIP60 antibody (Fig. 1A). In contrast, a similar analysis of H2A-binding proteins from irradiated cells did not show the presence of TIP60 (Fig. 1A). These findings suggest that TIP60 interacts specifically with H2AX in the nuclear soluble fraction after IR.

Previous studies have shown that K5 of histone H2A is acetylated by TIP60 in vitro (18). Because the K5 site is well conserved between H2AX and H2A, we examined K5 acetylation in immunoaffinity-purified H2AX by immunoblotting analysis using an anti-acetyl-H2A(K5) antibody. We found that H2AX(K5) was acetylated and that the amount of acetylated H2AX (Ac-H2AX) was substantially increased by IR (Fig. 1B). This finding was confirmed by MS-MS analysis (data not shown).

To confirm the role of TIP60 in H2AX acetylation, we constructed human GM02063 fibroblasts (51) that stably express TIP60 siRNA. In these cells, the amount of TIP60 protein was reduced by >80% (Fig. 1C). We then transiently transfected the cells with FLAG-H2AX, treated them with and without IR, and performed immunoprecipitation using an anti-FLAG antibody. Immunoblotting indicated that the DSB-induced acetylation of H2AX(K5) was significantly suppressed in TIP60 siRNA-expressing cells (Fig. 1D). Similar results were obtained using another TIP60-specific siRNA, confirming that the suppression of H2AX(K5) acetylation was due to the specific depletion of TIP60 (see Fig. S2A and B in the supplemental material). Moreover, the TIP60 complex directly acetylated free H2AX and H2AX in a nucleosomal context in vitro (data not shown). These results suggest that TIP60 is required for the acetylation of H2AX(K5) in the very early stages of the DNA damage response.

We next confirmed the DSB-induced interaction between H2AX and TIP60 by reciprocal affinity purification experiments using HeLa cells expressing FLAG-HA eTIP60. The TIP60 complex purified from the nuclear soluble fraction of irradiated cells included endogenous H2AX (Fig. 1E). Interestingly, immunoblot analysis using an anti-H2AX antibody revealed multiple higher-molecular-weight bands in addition to the band corresponding to H2AX. This finding indicated that TIP60-associated H2AX may contain modifications other than acetylation and phosphorylation following IR-induced DNA damage (Fig. 1E).

Acetylation by TIP60 is required for the ubiquitination of H2AX following DNA damage. The approximate molecular weight differences of the slower-migrating species led us to speculate that H2AX in the nuclear soluble fraction is polyubiquitinated upon DSBs. Immunoblotting of purified eH2AX from the soluble nuclear fraction revealed that multiple bands reacted with both anti-H2AX and antiubiquitin antibodies following IR (Fig. 2A). MS-MS analysis confirmed that the ~32-kDa protein was a form of eH2AX ubiquitinated on lysine 119 [Ub-eH2AX(K119)] (see Fig. S1B in the supplemental material). The DNA damage-dependent polyubiquitination of H2AX on K119 was further confirmed by eH2AX in which K119 was replaced with Arg [eH2AX(K119R)]. As expected, the DSB-induced polyubiquitination of eH2AX was significantly suppressed in eH2AX(K119R) mutant-expressing HeLa cells by immunoblotting analysis using anti-H2AX and antiubiquitin (FK2) antibodies (Fig. 2A). These results suggest that DSBs induce the polyubiquitination of H2AX at K119 in the nuclear soluble fraction of HeLa cells.

Because the TIP60 complex interacted with polyubiquitinated H2AX (poly-Ub-H2AX) after IR, we next examined the involvement of TIP60 in the polyubiquitination of H2AX in the nuclear soluble fraction. The specific depletion of TIP60 significantly suppressed the IR-induced polyubiquitination of eH2AX purified from the nuclear soluble fraction (Fig. 2A). We then analyzed whether TIP60 regulates the polyubiquitination of H2AX via the acetylation of K5 upon DNA damage. We expressed an eH2AX in which K5 was replaced with Arg [eH2AX(K5R)] in HeLa cells and then purified it by immunoaffinity chromatography from the nuclear soluble fraction of HeLa cells following treatment with or without IR. Immunoblotting analysis using anti-H2AX and antiubiquitin (FK2) antibodies revealed little or no increase in the level of polyubiquitinated eH2AX(K5R) after IR (Fig. 2A), suggesting that the DSB-induced polyubiquitination of H2AX in the nuclear soluble fraction requires TIP60-dependent acetylation.

The finding that TIP60 specifically interacts with H2AX and regulates its polyubiquitination in the nuclear soluble fraction following DNA damage suggests two possibilities. One is that TIP60 interacts with H2AX released from chromatin upon DNA damage. The other is that TIP60 is targeted to damaged chromatin and regulates the release of H2AX via histone modifications. To determine which of these possibilities is correct, we analyzed whether TIP60 regulates these H2AX modifications in the chromatin fraction. First, to examine the ubiquitination status of H2AX in the chromatin fraction, we performed anti-H2AX immunoblotting of the affinity-purified eH2AX from the chromatin fraction following treatment with or without IR. We found that eH2AX in the chromatin-bound

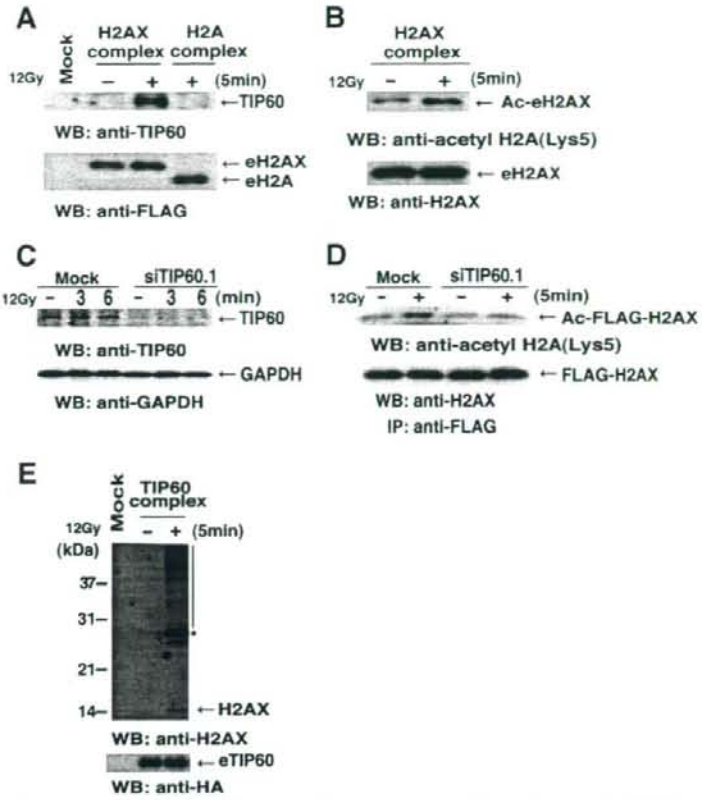

FIG. 1. TIP60 regulates the acetylation of H2AX(K5) upon DNA damage. (A) The mock control, eH2AX, and eH2A complexes were immunoaffinity purified from the nuclear soluble fraction of HeLa cells treated without (−) or with (+) IR at 12 Gy followed by a 5-min recovery. Immunoblotting analysis was performed with anti-TIP60 (top) and anti-FLAG (bottom) antibodies. (B) The eH2AX complex immunoaffinity purified from the nuclear soluble fraction of HeLa cells treated with IR (12 Gy) followed by a 5-min recovery. Proteins were analyzed by immunoblotting using anti-acetyl-K5 of H2A antibody (top). Unirradiated cells (−) were used as controls. eH2AX was used as a loading control (bottom). (C) Depletion of TIP60 by TIP60 siRNA. Shown are anti-TIP60 immunoblots of lysates from TIP60 siRNA (siTIP60.1)-expressing and mock control cells prepared at the indicated times after IR at 12 Gy (top). GAPDH was used as a loading control (bottom). (D) Effect of the depletion of TIP60 on the acetylation of H2AX after IR. TIP60-specific siRNA (siTIP60.1)-expressing and mock control cells transfected with a FLAG-H2AX expression vector were treated with IR at 12 Gy and allowed to recover for 5 min. Immunoprecipitation was carried out using the anti-FLAG antibody, and proteins were analyzed by immunoblotting with antibodies against H2A acetylated on K5 (top) or total H2AX (bottom). Cells were treated with sodium butyrate (final concentration, 5 mM) for the detection of acetylation. (E) Western blot analysis of the TIP60 complex by use of anti-H2AX (top) and anti-HA (bottom; loading control) antibodies. Shown are the mock control and the TIP60 complex immunoaffinity purified from nuclear extract of HeLa cells stably expressing FLAG-HA eTIP60 with IR at 12 Gy followed by a 5-min recovery. Bands that reacted with anti-H2AX antibody are indicated by an asterisk and a bar. eTIP60 was used as a loading control (bottom). WB, Western blot.

fraction was monoubiquitinated under normal conditions, as reported previously (Fig. 2B and C) (61). The level of monoubiquitination of eH2AX was increased following IR (Fig. 2B and C). Importantly, eH2AX was significantly polyubiquitinated following IR (Fig. 2C). The DSB-induced poly- and monoubiquitination of eH2AX in the chromatin fraction were abolished by the K119R mutation [eH2AX(K119R)] (Fig. 2B and C). We further confirmed these findings by a coimmunoprecipitation (coIP) experiment using 293T cells expressing FLAG-tagged H2AX(K119R) and HA-tagged ubiquitin (see Fig. S3A in the supplemental material). These results indicate that eH2AX in the chromatin fraction was mono- and polyubiquitinated at K119 following IR. However, we cannot exclude the possibility that H2AX is also ubiquitinated independent of DNA damage at a residue other than K119, because a longer exposure of the anti-H2AX immunoblot of the K119R mutant suggested weak monoubiquitination after IR.

We next examined the involvement of TIP60 in the DSB-induced modifications of H2AX in the chromatin fraction. The depletion of TIP60 in HeLa cells by use of TIP60 siRNA repressed the DSB-induced mono- and polyubiquitination of eH2AX (Fig. 2C). Monoubiquitination of eH2AX and H2AX in the chromatin fraction under normal conditions was not disturbed by the depletion of TIP60 (Fig. 2C). These findings are consistent with the notion that TIP60 regulates the DSB-induced mono- and polyubiquitination of H2AX in the chro-

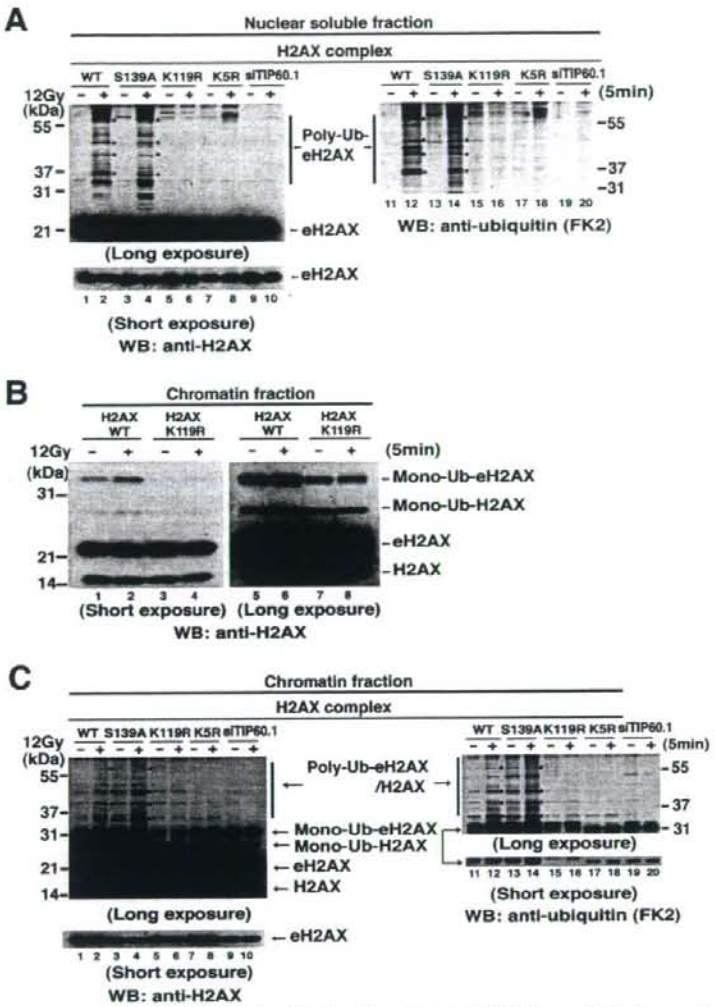

FIG. 2. Acetylation of H2AX regulated by TIP60 is required for the ubiquitination of H2AX upon DNA damage. (A and C) Wild-type eH2AX (lanes 1, 2, 11, and 12) and mutants eH2AX(S139A) (lanes 3, 4, 13, and 14), eH2AX(K119R) (lanes 5, 6, 15, and 16), and eH2AX(K5R) (lanes 7, 8, 17, and 18) were immunoaffinity purified from the nuclear soluble (A) and chromatin (C) fractions of cells stably expressing wild-type or mutant forms of eH2AX treated with IR (12 Gy) followed by a 5-min recovery. Wild-type eH2AX was also purified from TIP60 knockdown cells (siTIP60.1) expressing wild-type eH2AX (lanes 9, 10, 19, and 20). Proteins were analyzed by immunoblotting using anti-H2AX (left) and anti-ubiquitin (FK2) (right) antibodies. Asterisks indicate that the signals reacted with both anti-H2AX and antiubiquitin (FK2) antibodies. eH2AX was used as a loading control (bottom). (A) Unmodified eH2AX and polyubiquitinated eH2AX (poly-Ub-eH2AX) are indicated. (B) The monoubiquitination status of immunoaffinity-purified wild-type eH2AX (lanes 1, 2, 5, and 6) and the K119R mutant (lanes 3, 4, 7, and 8) from the chromatin fractions of cells treated with IR (12 Gy) followed by a 5-min recovery was analyzed by immunoblotting using anti-H2AX antibody. Unmodified eH2AX and mono-Ub-eH2AX were detected together with unmodified H2AX and mono-Ub-H2AX. (C) Poly-Ub-eH2AX and endogenous H2AX are indicated. WT, wild type; WB, Western blot.

matin fraction. Because the IR-induced acetylation was abolished by the eH2AX(K5R) mutation in the chromatin fraction (Fig. 3), we concluded that H2AX(K5) is the target of acetylation upon DSBs in the chromatin and nuclear soluble fractions. Importantly, DSB-induced mono- and polyubiquitination of eH2AX were significantly repressed by the eH2AX(K5R) mutation in the chromatin fraction as in the nuclear soluble fraction of HeLa cells (Fig. 2C). The requirement for acetylation in the DSB-induced mono- and polyubiquitination of H2AX was confirmed by a coIP experiment using 293T cells expressing FLAG-tagged H2AX (K5R) and HA-tagged ubiquitin (see Fig. S3A in the supplemental material). Taken together, these findings suggest that TIP60 regulates the DSB-induced mono- and polyubiq-

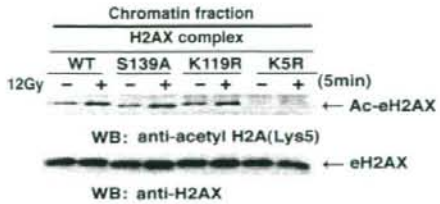

FIG. 3. H2AX is acetylated independent of phosphorylation and ubiquitination upon DNA damage. Wild-type and mutant eH2AX proteins (S139A, K119R, and K5R) were immunoaffinity purified from the chromatin fraction of HeLa cells treated with IR at 12 Gy followed by a 5-min recovery, and the acetylation status was analyzed by immunoblotting with the anti-acetyl-K5 of H2A (top). eH2AX was used as a loading control (bottom). Cells were treated with sodium butyrate (final concentration, 5 mM) for the detection of acetylation. WT, wild type; WB, Western blot.

uitination of H2AX in the chromatin fraction. If preexisting monoubiquitinated H2AX (mono-Ub-H2AX) in the chromatin fraction is the only source for DSB-induced polyubiquitination, the amount of mono-Ub-H2AX should be decreased. However, because the amount of mono-Ub-H2AX was increased upon DNA damage (Fig. 2C; also see Fig. S3A in the supplemental material), DNA damage can induce the de novo polyubiquitination of H2AX in the chromatin fraction by TIP60.

To confirm the connection between acetylation and polyubiquitination, we examined the time courses of the H2AX modifications in the chromatin fraction of HeLa cells after IR. The polyubiquitination of eH2AX peaked sharply 2 to 5 min after IR and nearly paralleled its acetylation (Fig. 4A and B). The increase in mono-Ub-H2AX also peaked at 2 to 5 min (Fig. 4B). We also obtained comparable results in a coIP experiment using 293T cells expressing FLAG-tagged H2AX and HA-tagged ubiquitin (see Fig. S3B in the supplemental material). The similarities in the kinetics of acetylation and of the mono- and polyubiquitination of H2AX strongly suggest a preferential linkage of acetylation with de novo polyubiquitination of eH2AX in the chromatin fraction immediately after IR. Notably, the ratio of polyubiquitination to monoubiquitination of H2AX in the nuclear soluble fraction is much higher than that in the chromatin fraction. This suggests that the polyubiquitination but not the monoubiquitination of H2AX is involved in the release of H2AX from chromatin upon DNA damage. Collectively, these findings suggest that TIP60 facilitates H2AX release upon DNA damage via acetylation-dependent polyubiquitination of H2AX at the very early stage of DNA repair.

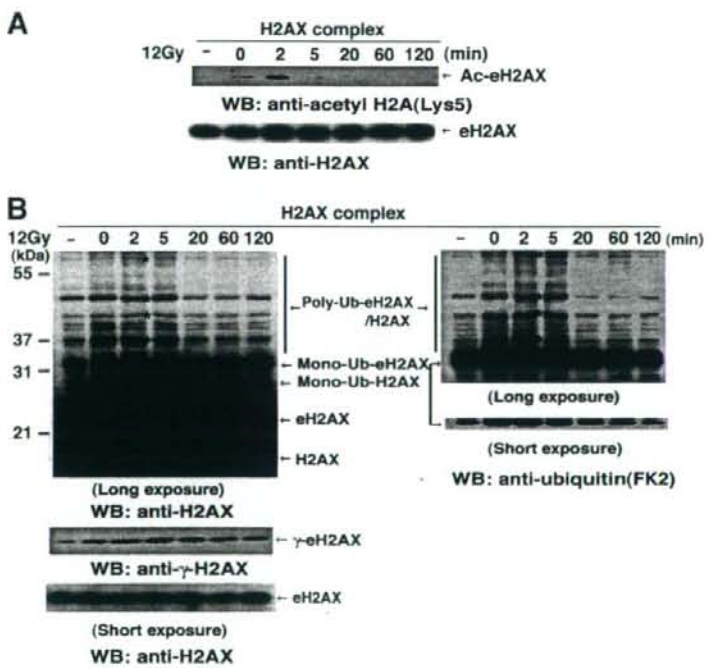

FIG. 4. Time course of acetylation, ubiquitination, and phosphorylation of H2AX after induction of DSBs. Wild-type eH2AX was immunoaffinity purified from the chromatin-bound fraction derived from HeLa cells stably expressing eH2AX at the indicated times of recovery after IR (12 Gy). (A) The acetylation status was analyzed by immunoblotting with the anti-acetyl-K5 of H2A (top). eH2AX was used as a loading control (bottom). Cells were treated with sodium butyrate (final concentration, 5 mM) for the detection of acetylation. (B) Proteins were analyzed by immunoblotting using anti-H2AX (top and bottom in left gel), anti-γ-H2AX (middle in left gel), and antiubiquitin (FK2) (right) antibodies. eH2AX was used as a loading control (bottom in left gel). Asterisks indicate the bands reacted with both anti-H2AX and antiubiquitin (FK2) antibodies. WB, Western blot.

Acetylation-dependent ubiquitination of H2AX upon DNA damage is independent of phosphorylation. The above data provide evidence for the acetylation-dependent ubiquitination of H2AX upon DSBs by TIP60. However, the relationship between the DSB-induced acetylation-dependent ubiquitination and phosphorylation of H2AX remains unclear. To investigate this further, we examined the modification status of a phosphorylation mutant of H2AX [eH2AX(S139A)] after IR. Immunoblotting analysis using anti-H2AX and antiubiquitin (FK2) antibodies revealed that eH2AX(S139A) affinity purified from both the nuclear soluble and chromatin fractions were mono- and polyubiquitinated following IR (Fig. 2A and C). This finding was supported by a coIP experiment using 293T cells expressing FLAG-tagged H2AX(S139A) and HA-tagged ubiquitin (see Fig. S3A in the supplemental material). Moreover, eH2AX(S139A) in the chromatin fraction was acetylated after IR (Fig. 3). These findings suggest that phosphorylation is not required for either acetylation or ubiquitination after IR. Consistently, in contrast to what was seen for the acetylation and polyubiquitination of eH2AX, which peaked 2 to 5 min after IR, the level of phosphorylation was constant during the experiment (Fig. 4B). Taken together, these results indicated that acetylation-dependent ubiquitination is regulated independently of the phosphorylation of H2AX upon DNA damage.

To determine the biological consequences of the acetylation, ubiquitination, and phosphorylation of H2AX following DNA damage, we established HeLa cells expressing siRNAs targeted to the noncoding region of the endogenous H2AX for the reconstitution experiments with the expression of H2AX mutants (see Fig. S4A in the supplemental material). The expression of the GFP-H2AX wild type and GFP-H2AX mutants was not affected by the coexpression of H2AX siRNA (see Fig. S4A in the supplemental material). We found that following IR, the survival of HeLa cells expressing H2AX(K5R), H2AX(K119R), or H2AX(S139A) mutants was reduced compared to that seen for H2AX knockdown HeLa cells expressing wild-type eH2AX or for the parental HeLa cells ($P < 0.01$) (see Fig. S4B in the supplemental material). These data suggest that along with H2AX phosphorylation, H2AX acetylation and ubiquitination play a significant role in cellular survival following DNA damage.

The TIP60-UBC13 complex regulates the DSB-induced ubiquitination of H2AX. In our previous study, we suggested that UBC13 can regulate the ubiquitination of H2AX after IR (64). Indeed, we found that UBC13 is included in eH2AX complexes that were affinity purified from either nuclear soluble or chromatin fractions and that the amount of UBC13 in the H2AX complexes was substantially increased following IR (Fig. 5A). We further analyzed the localization of GFP-tagged TIP60 or UBC13 expressed in GM02063 cells carrying DSBs along a microirradiated line. We found that both GFP-TIP60 and GFP-UBC13 accumulated at damaged sites 5 min after microirradiation (Fig. 5B). We confirmed that the integration of UBC13 into TIP60 purified from the nuclear soluble fraction is stimulated following IR (Fig. 5C). The ubiquitination of H2AX after the induction of DSBs was disturbed in the UBC13-depleted HeLa cells expressing UBC13 siRNA, confirming the direct dependence of the ubiquitination of H2AX on UBC13 in the DNA damage response (Fig. 5D; also see Fig. S5 in the supplemental material). Collectively, these findings indicate that TIP60 interacts with UBC13 to facilitate the ubiquitination of H2AX in damaged chromatin.

H2AX is released from damaged chromatin after induction of DSBs. Following IR, the level of poly-Ub-H2AX appeared to increase more in the soluble nuclear fraction than in the chromatin-bound fraction (Fig. 2A and C). This indicated that a fraction of H2AX may undergo dynamic release from damaged chromatin. To examine the mobility of DSB-associated H2AX, we utilized a laser UVA microirradiation system to induce DSBs at the single-cell level (21, 51, 58). We first confirmed that H2AX is poly- and monoubiquitinated after the induction of DSBs by UV irradiation of bromodeoxyuridine-labeled cells (data not shown). We then performed photobleaching analysis to assess histone binding properties in vivo following the induction of DSBs with the laser UVA microirradiation system (20, 24, 27). We confirmed that the stably expressed GFP-H2AX proteins in HeLa and GM02063 cells share a range of physiological properties with the endogenous histone: GFP-H2AX was found to localize in chromatin throughout the cell cycle, similar to other histones, and the salt extraction profile was similar to that of the endogenous H2AX (data not shown) (44). We then performed iFRAP analysis (14, 37) of GFP-H2AX in combination with microirradiation to determine whether GFP-H2AX is released from damaged chromatin. In iFRAP experiments, immediately following microirradiation, all of the fluorescence (except in small regions of irradiated areas and in unirradiated areas) was bleached, and the remaining GFP-H2AX fluorescence was chased using LSM510 confocal microscopy. As a result, the remaining GFP-H2AX fluorescence within the irradiated area became significantly weaker than that in the unirradiated area (Fig. 6A and B), suggesting that GFP-H2AX can diffuse from chromatin only in the irradiated area. Thus, DNA damage provokes the release of GFP-H2AX from chromatin.

The dynamics of H2AX following DNA damage were examined by determining the fluorescence recovery of GFP-H2AX within two independent strips of a single nucleus, one in the irradiated area and the other in an unirradiated region, immediately following microirradiation (Fig. 6C). Rapid fluorescence recovery was observed in the irradiated region (27.6% ± 8.2% at 260 s), whereas the fluorescence intensity in the unirradiated region did not change much during the observed time (5.0% ± 4.3% at 260 s) ($P < 0.000001$) (Fig. 6D; also see the video in the supplemental material). These findings also indicate that the fluorescence recovery in the irradiated region is due to the unbleached GFP-H2AX molecules released from damaged chromatin, because GFP-H2AX in the unirradiated area showed stable binding to chromatin (Fig. 6C and D). As a control, we observed that GFP-H2A in the irradiated area displays a recovery of fluorescence intensity slower (13.3% ± 8.4% at 260 s) than that of GFP-H2AX ($P < 0.0005$) (Fig. 6E).

Chromatin has been shown to move in response to DNA damage (4, 21). We quantified the dynamics of other core histones following DNA damage to determine whether this occurred. GFP-tagged H2B (18.3% ± 9.9% at 260 s), H3 (11.4% ± 6.9% at 260 s), and H4 (10.0% ± 4.3% at 260 s) displayed slower recoveries of fluorescence than GFP-H2AX following the induction of DNA damage ($P < 0.005$) (see Fig. S6 in the supplemental material). We noted that irradiation

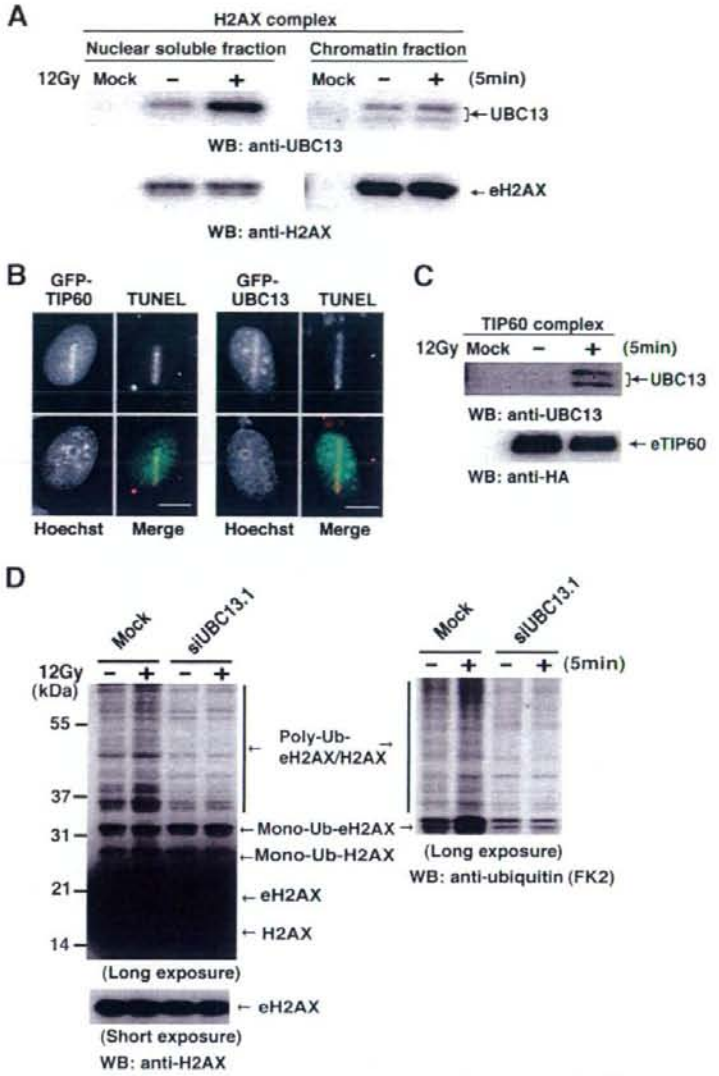

FIG. 5. UBC13, a ubiquitin-conjugating enzyme, interacts with TIP60 in damaged chromatin. (A) Affinity purification of eH2AX from the nuclear soluble (left) and chromatin (right) fractions of HeLa cells treated with IR at 12 Gy followed by a 5-min recovery. As a control, a mock purification was performed using nontransfected HeLa cells. UBC13 was detected by immunoblotting using anti-UBC13 antibody (top). eH2AX was used as a loading control (bottom). (B) Accumulation of GFP-TIP60 (left) or GFP-UBC13 (right) in GM02063 cells at sites containing DSBs after a 5-min recovery from laser UVA microirradiation. TUNEL staining was performed to detect DSBs induced by microirradiation. GFP-TIP60/UBC13 and TUNEL signals are shown in green and red, respectively, in merged images. Scale bars, 10 μm. (C) DSBs facilitate the interaction of UBC13 with the TIP60 complex. Immunoblot analysis of the mock control and the TIP60 complex affinity purified from the nuclear soluble fraction of cells treated with IR (12 Gy) followed by a 5-min recovery using anti-UBC13 antibody (top). eTIP60 was used as a loading control (bottom). (D) Wild-type eH2AX was affinity purified from the chromatin fraction of UBC13-specific siRNA (siUBC13.1)-expressing cells or the mock control cells treated with IR (12 Gy) followed by a 5-min recovery. Proteins were analyzed by immunoblotting using anti-H2AX (left) and antiubiquitin (FK2) (right) antibodies. WB, Western blot.

only subtly affected the recovery rate of the fluorescence intensity of H2B-GFP, which is the dimerization partner for all H2A variants, including H2AX. Because H2AX accounts for only 5 to 10% of the total H2A in chromatin, the DSB-induced release of H2AX may have a limited impact on the global dynamics of total H2B. Fluorescence recovery rates reflect the amount of fluorescence molecules coming into the photobleached area. Therefore, the high fluorescence recovery rate of GFP-H2AX compared to those of other GFP-tagged core histones strongly suggests the release of GFP-H2AX molecules